PROCEEDINGS OF SCIENCE

Flavor Diagonal Nucleon Charges

Sungwoo Park,[a,b,c,*] **Tanmoy Bhattacharya,**[a] **Rajan Gupta,**[a] **Huey-Wen Lin,**[e] **Santanu Mondal,**[a,e] **Boram Yoon**[d] **and Rui Zhang**[e]

[a] *Theoretical Division T-2, Los Alamos National Laboratory, Los Alamos, NM 87545, USA*
[b] *Center for Nonlinear Studies, Los Alamos National Laboratory, Los Alamos, NM 87545, USA*
[c] *Thomas Jefferson National Accelerator Facility, 12000 Jefferson Avenue, Newport News, VA 23606, USA*
[d] *Computer, Computational and Statistical Science Division CCS-7, Los Alamos National Laboratory, Los Alamos, NM 87545, USA*
[e] *Department of Physics and Astronomy, Michigan State University, East Lansing, MI 48824, USA*
E-mail: sungwoo@jlab.org, rajan@lanl.gov, tanmoy@lanl.gov, santanu@lanl.gov, boram@lanl.gov, hueywen@msu.edu, zhangr60@msu.edu

This talk provides an update on the calculation of matrix elements of flavor diagonal axial, scalar and tensor quark bilinear operators between the nucleon ground state. The simulations are done using Wilson-clover fermions on a sea of eight 2+1+1-flavor HISQ ensembles generated by the MILC collaboration. We discuss the signal in the connected and disconnected contributions, calculation of the renormalization constants and mixing in the RI-sMOM scheme, and control over the simultaneous chiral-continuum-finite-volume fit used to extract the final charges.

The 38th International Symposium on Lattice Field Theory, LATTICE2021 26th-30th July, 2021
Zoom/Gather@Massachusetts Institute of Technology

*Speaker

PoS(LATTICE2021)558

1. Introduction

Results for the matrix elements of flavor diagonal axial, scalar and tensor quark bilinear operators between the nucleon ground state provide a number of quantities of phenomenological interest. The axial charges give contribution of each quark flavor to the spin of the nucleon and the spin dependent interaction of dark matter with nuclear targets; the tensor charges give the contribution of the quark electric dipole moment (EDM) operator to the nucleon EDM and the zeroth moment of transversity distribution of quarks in nucleons; and the flavor diagonal scalar charges give the pion-nucleon sigma term, strangeness content of the nucleon, the strength of the spin-independent coupling of dark matter to nucleons, and enters in the search for BSM physics such as in $\mu \rightarrow e$ conversion. This talk presents the status of our calculations of these matrix elements on eight 2+1+1-flavor HISQ ensembles generated by the MILC collaboration [1] using Wilson-clover valence fermions with quark masses tuned to reproduce the sea M_π and $M_{s\bar{s}}$ values. The parameters of these ensembles are given in Table 1. This set includes one physical $M_\pi \approx 138$ MeV ensemble (labeled as $a09m130$) at $a \approx 0.09$ fm and $M_\pi L \approx 3.9$.

All results presented here should be considered preliminary unless otherwise stated. They are updates on results for $g^q_{A,T}$ in Refs. [2–4], and for g^q_S in Ref. [5]. In addition to nucleon 2-point functions, we calculate the connected [2] and disconnected [3, 4] contributions to 3-point functions illustrated in the two left panels in Fig. 1(a), and the analogous quark level diagrams in Landau gauge for calculating the renormalization constants in the RI-sMOM scheme Fig. 1(b).

Ensemble ID	a (fm)	M_π (MeV)	$M_\pi L$	$L^3 \times T$	N^l_{conf}	N^l_{src}	N^s_{conf}	N^s_{src}	$N_{\text{LP}}/N_{\text{HP}}$
$a15m310$	0.1510(20)	320(5)	3.93	$16^3 \times 48$	1917	2000	1917	2000	50
$a12m310$	0.1207(11)	310(3)	4.55	$24^3 \times 64$	1013	10000	1013	8000	50
$a12m220$	0.1184(10)	228(2)	4.38	$32^3 \times 64$	958	11000	870	5000	30–50
$a09m310$	0.0888(8)	313(3)	4.51	$32^3 \times 96$	1017	10000	889	6000	50
$a09m220$	0.0872(7)	226(2)	4.79	$48^3 \times 96$	712	8000	847	10000	30–50
$a09m130$	0.0871(6)	138(1)	3.90	$64^3 \times 96$	1270	10000	541	10000	50
$a06m310$	0.0582(4)	320(2)	3.90	$48^3 \times 144$	808	12000	948	10000	50
$a06m220$	0.0578(4)	235(2)	4.41	$64^3 \times 144$	1001	10000	1002	10000	50

Table 1: Update from Refs. [3, 4] of the statistics and 2+1+1-flavor HISQ ensembles used for the calculation of disconnected contributions. Statistics for the connected are the same as in Ref. [2]. $N^{l,s}_{\text{conf}}$ is the number of gauge configurations analyzed for light (l) and strange (s) flavors. $N^{l,s}_{\text{src}}$ is the number of random sources used per configurations, and $N_{\text{LP}}/N_{\text{HP}}$ is the ratio of low/high precision meausurements.

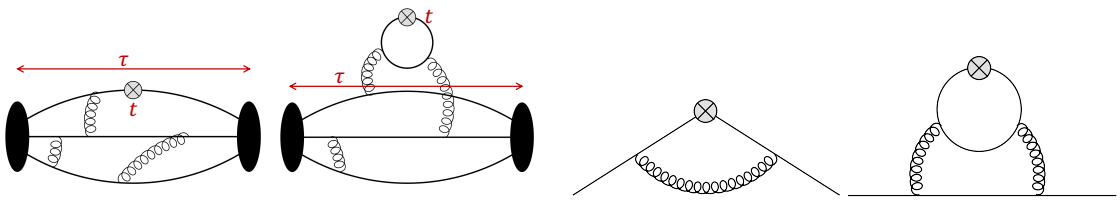

(a) Nucleon charges (b) NPR

Figure 1: The connected and disconnected diagrams calculated (i) for flavor diagonal nucleon charges, and (ii) non-perturbative renormalization in the RI-sMOM scheme using quark states in Landau gauge.

2. Details of 2-point and 3-point function analysis

Details of the calculations of the quark propagators on HYP smeared lattices using Wuppertal smearing are given in Ref. [2]. The nucleon interpolating operator used both at the source and the sink in all calculations is $\mathcal{N}(x) = \epsilon^{abc}\left[q_1^{aT}(x)C\gamma_5\frac{(1\pm\gamma_4)}{2}q_2^b(x)\right]q_1^c(x)$. All 3-point functions are calculated with zero momentum operator insertion and the nucleon state at the sink is also projected to zero momentum. From these we get forward matrix elements from which charges are obtained.

The nucleon spectrum is obtained from the 2pt function, with spin projection $(1+\gamma_4)/2$, fit using the spectral decomposition truncated at four states,

$$C^{\rm 2pt}(\tau) = \sum_{i=0} |\mathcal{A}_i|^2 e^{-M_i\tau}. \tag{1}$$

We carry out two types of analyses: The "standard" fit uses wide priors for all the excited-state amplitudes, $\mathcal{A}_i$, and masses, M_i, i.e., the priors are only used to stabilize the fits. This is called the $\{4\}$ or "standard" strategy. (ii) A narrow prior for M_1 with central value given by the non-interacting energy of the lowest allowed $N\pi$ or $N\pi\pi$ state is used. This is called the $\{4^{N\pi}\}$ strategy. The resulting values of $\mathcal{A}_0$ and the M_i are used as inputs in the analysis of the 3-point functions. The mass gap, $M_1 - M_0$, in the 2 analyses is significantly different, however the augmented χ^2 minimized in the fits is essentially the same. Thus, the two strategies are not distinguished on the basis of our fits and we examine the senstivity of the results for the charges to the two M_1.

The nucleon 3pt function at zero momentum, in our setup, is given by

$$C_\Gamma^{\rm 3pt}(t;\tau) = {\rm Tr}[P_\Gamma\langle 0|\mathcal{N}(\tau)O_\Gamma(t,\mathbf{q}=0)\bar{\mathcal{N}}(0,\mathbf{p}=0)|0\rangle]\,, \tag{2}$$

where the operator $O_\Gamma^q = \bar{q}\Gamma q$, $q\in\{u,d,s\}$, and $P_\Gamma = (1+\gamma_4)(1+i\gamma_5\gamma_3)/2$ is the spin projection used for forward propagating nucleons. This P_Γ singles out direction "3", while "1" and "2" are equivalent under the cubic rotational symmetry. Flavor diagonal 3pt functions require the sum of connected (conn) and disconnected (disc) contributions illustrated in Fig. 1(a):

$$C_\Gamma^{\rm 3pt}(t;\tau) = C_\Gamma^{\rm conn}(t;\tau) + C_\Gamma^{\rm disc}(t;\tau). \tag{3}$$

For the scalar case, the disconnected contribution is calculated using the vacuum subtracted operator $O_S^q - \langle O_S^q\rangle$. The calculation of the quark loop with zero-momentum operator insertion is estimated stocastically using Z_4 random noise sources as explained in Ref. [6].

We analyze the zero-momentum nucleon 3pt function (sum of connected and disconnected diagram contributions) using the spectral decomposition

$$C_\Gamma^{\rm 3pt}(\tau;t) = \sum_{i,j=0} \mathcal{A}_i\mathcal{A}_j^*\langle i|O_\Gamma|j\rangle e^{-M_i t - M_j(t-\tau)}, \tag{4}$$

and obtain the bare charges, $g_\Gamma^{q;\rm bare}$, from the ground state matrix elements $\langle 0|O_\Gamma|0\rangle$. The challenge is removing excited state contributions (ESC) which are observed to be large at source-sink separation $\tau\approx 1.4$ fm, the typical distance beyond which the signal degrades due to the $e^{(M_N-3/2M_\pi)\tau}$ increase in noise. With the current statistics, we are only able to keep one excited state in the analysis using Eq. (4) and fits leaving M_1 a free parameter are not stable. Thus we take M_1 from fits to the 2-point function, i.e., we analyze the data with the two strategies, $\{4\}$ and $\{4^{N\pi}\}$.

A challenge to distinguishing between $\{4\}$ and $\{4^{N\pi}\}$ strategies is that the difference in the corresponding M_1 becomes significant only for $M_\pi \lesssim 200$ MeV, which in our setup means only in the $a091m130$ ensemble. Previous work shows that the difference in axial and tensor charges, $g_{A,T}$, is small [2]. For the isoscalar scalar charge g_S^{u+d}, χPT suggests a large contribution from $N\pi$ and $N\pi\pi$ states leading to a large difference in the value of the pion-nucleon sigma term as explained in Ref. [5]. To understand and quantify these differences we do the full analysis with both strategies.

Note that in our previous works [3, 4], the fits to remove ESC in $C_\Gamma^{\rm conn}(t;\tau)$ and $C_\Gamma^{\rm disc}(t;\tau)$ were done separately, as was the chiral-continuum (CC) extrapolations of $g_\Gamma^{q,\rm disc}$ and $g_\Gamma^{q,\rm conn}$. This introduces an unquantified systematic [4] that has now been removed by fitting to $C_\Gamma^{\rm conn}(t;\tau) + C_\Gamma^{\rm disc}(t;\tau)$ and extrapolating g_Γ^q.

3. Renormalization

We have now explicitly evaluated the 3×3 flavor mixing matrices in $\overline{\rm MS}$ scheme at 2 GeV to get the renormalized flavor diagonal axial, scalar and tensor charges. The corrections are small for axial and tensor charges as anticipated in [3, 4], but significant for the scalar operators. For example, g_S^s gets about $6\sim 20\%$ correction to the diagonal term $Z_S^{s,s} g_S^s$ from $Z_S^{s,u+d} g_S^{u+d,\rm bare}$ [7].

For $N_f = 2{+}1$-flavor theory, the mixing matrix for bilinear operators O_Γ^f, $f\in\{u-d, u{+}d, s\}$ is

$$Z_\Gamma^{\text{RI-sMOM}} = \begin{pmatrix} Z_\Gamma^{u-d,u-d} & 0 & 0 \\ 0 & Z_\Gamma^{u+d,u+d} & Z_\Gamma^{u+d,s} \\ 0 & Z_\Gamma^{s,u+d} & Z_\Gamma^{ss} \end{pmatrix} = \begin{pmatrix} c_l & 0 & 0 \\ 0 & c_l - 2d_{ll} & -2d_{sl} \\ 0 & -d_{ls} & c_s - d_{ss} \end{pmatrix}^{-1} \tag{5}$$

where c_f and $d_{ff'}$ are the projected amputated Green's function for the connected and disconnected contributions (Fig. 1(b)) respectively. They are defined as follows,

$$c_f^\Gamma \equiv \frac{1}{Z_\psi^f}\text{Tr}[P_\Gamma^{\text{RI-sMOM}}\langle f|O_\Gamma^f|f\rangle_{\rm conn}]\,, \tag{6}$$

$$d_{ff'}^\Gamma \equiv \frac{-1}{Z_\psi^f}\text{Tr}[P_\Gamma^{\text{RI-sMOM}}\langle f|O_\Gamma^{f'}|f\rangle_{\rm disc}]\,, \tag{7}$$

with Z_ψ^f the wave function renormalization, $P_\Gamma^{\text{RI-sMOM}}$ the projector for the RI-sMOM scheme, and $\langle f|O_\Gamma^f|f\rangle$ the amputated Green's functions. The quark loop is again estimated stochastically. From Eq. (5), we can calculate each $Z_\Gamma^{\text{RI-sMOM}}(q^2)$ from the associated 2 connected (c_l^Γ, c_s^Γ) and 4 disconnected (d_{ll}^Γ, d_{ls}^Γ, d_{sl}^Γ, d_{ss}^Γ) projected amputated Green's functions. Here q^2 is the momentum flowing in all three legs and defines the RI-sMOM scale. The matrix $Z_\Gamma^{\text{RI-sMOM}}(q^2)$ is roughly diagonal since $c_l^\Gamma \sim O(1)$ but $d_{ff'}^\Gamma$ are a few percent at $|q|\sim 2$ GeV for the scalar operator, and smaller still for the axial and tensor operators.

The four steps to get $Z_\Gamma^{\overline{\rm MS}}(\mu = 2\text{ GeV})$ are: (i) from the 2 c_f^Γ and 4 $d_{ff'}^\Gamma$, we calculate the full 3×3 matrix $Z_\Gamma^{\text{RI-sMOM}}(q^2)$ for various q^2 using Eq. (5). (ii) Perform horizontal matching to $\overline{\rm MS}$, $Z_\Gamma^{\overline{\rm MS}}(\mu) = C_\Gamma^{RI\to\overline{\rm MS}}(\mu) Z_\Gamma^{\text{RI-sMOM}}(|q|)$, at scale $\mu = |q|$ using perturbation theory for $C_\Gamma^{RI\to\overline{\rm MS}}(\mu)$. (iii) Perturbative running in $\overline{\rm MS}$ to fixed scale 2GeV, $Z_\Gamma^{\overline{\rm MS}}(2GeV;\mu) = C_\Gamma^{\overline{\rm MS}}(2GeV,\mu) Z_\Gamma^{\overline{\rm MS}}(\mu)$. (iv) Remove dependence on $\mu^2 = q^2$ artifacts using the fit $Z_\Gamma^{\overline{\rm MS}}(2GeV;\mu) = Z_\Gamma^{\overline{\rm MS}}(2GeV) + c_1\mu^2 + c_2\mu^4$.

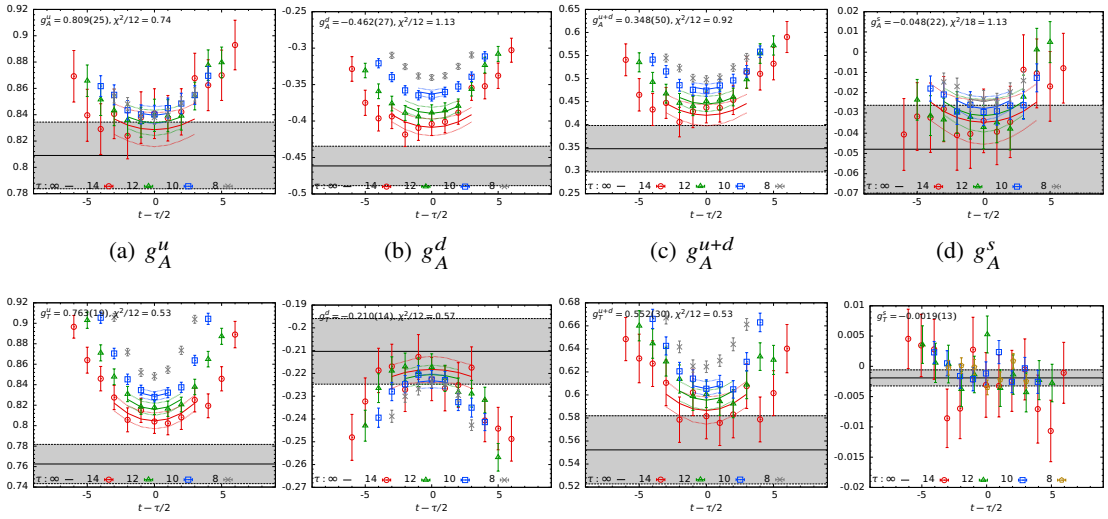

(a) g_A^u (b) g_A^d (c) g_A^{u+d} (d) g_A^s

(e) g_T^u (f) g_T^d (g) g_T^{u+d} (h) g_T^s

Figure 2: Results of bare g_A (top) and g_T (bottom) from the fits to the sum of the connected and disconnected data plotted versus $(t-\tau/2)/a$ for the physical M_π ensemble $a09m130$. Result of the fit is shown by lines of the same color as the data for various τ/a listed in the label, and the $\tau \to \infty$ is given by the gray band.

	g_A^u	g_A^d	g_A^s	g_T^u	g_T^d	g_T^s
This work (preliminary)	0.775(18)	-0.453(15)	-0.038(7)	0.746(18)	-0.196(8)	-0.0015(8)
PNDME 18 [3, 4]	0.777(39)	-0.438(35)	-0.053(8)	0.784(30)	-0.204(15)	-0.0032(7)

Table 2: Preliminary estimates of flavor diagonal axial and tensor charges compared with our previous results, PNDME 18, from Refs. [3, 4]. The errors quoted under "This work" are only statistical.

4. Results for $g_{A,S,T}$

The data for $C_\Gamma^{\rm conn}(t;\tau) + C_\Gamma^{\rm disc}(t;\tau)$ are more noisy than $C_\Gamma^{\rm conn}(t;\tau)$, so we are only able to include two states (ground plus one excited) when removing ESC using Eq. (4). In some cases that show no obvious τ dependence, and the preliminary values here are the unweighted average of central 5–6 points in the 3pt/2pt ratio to get g_T^s. Examples of ESC fits are shown in Figs. 2 and 3. The chiral-continuum (CC) fits to the renormalized charges are shown in Figs. 4, 5, 6 and 7. Possible finite-volume corrections are ignored. The final results are summarized in Tables 2, 3 and 4. Some details are as follows:

Axial charges, $g_A^{u,d,u+d,s}$: We quote results of 2-state fit to the data from the "standard" analysis of ESC. The data are noisy and do not show clear τ dependence for $q = u, s$ on the $a \approx 0.12$ and 0.15 fm ensembles. The ESC in both g_A^u and g_A^d reduces g_A^{u+d}, with that in g_A^d being larger (see Figs. 2). Adding results of separate fits to g_A^u and g_A^d gives values consistent with those from a single fit to g_A^{u+d}. The CC extrapolations are shown in Fig. 4. Both g_A^u and g_A^d show similar depencence on a and M_π. There is a significant slope versus M_π^2. The g_A^s data show a small dependence on a and M_π. The final extrapolated g_A^q are summarized in the Table 2. Results for $g_A^{u,d}$ are consistent with those in Ref. [4], while g_A^s is $\approx 2\sigma$ smaller.

Tensor charges, $g_T^{u,d,u+d,s}$: Quoted results are from the "standard" analysis of ESC with 2-state fit to $C_T^{3\text{pt},u}(t,\tau)$ and $C_T^{3\text{pt},d}(t,\tau)$. The ESC in g_T^u reduces while that in g_T^d increases g_T^{u+d}. The magnitude of ESC in g_T^u is larger. Again, combining results of separate fits to g_T^u and g_T^d gives values consistent with results of fits to g_T^{u+d}. As shown in Fig. 2(h) and Ref. [3], there is no clear ESC pattern in $C_T^{3\text{pt},s}(t;\tau)$, and the preliminary values here are the unweighted average of central points in the 3pt/2pt ratio to get g_T^s. The CC fits are shown in Fig. 5, and the final extrapolated g_T^q are summarized in the Table 2. Estimates of $g_T^{u,d}$ are consistent with Ref. [3], while again g_T^s is smaller.

Scalar charges $g_S^{u,d,u+d,s}$ **and the pion-nucleon sigma term** $\sigma_{\pi N}$: Chiral PT analyses provide two differences in the chiral behavior of flavor diagonal scalar charges. First, the CC ansatz $d_0 + d_a a + d_1 M_\pi + d_2 M_\pi^2 + d_{2L} M_\pi^2 \log M_\pi^2$ has the chiral behavior starting with a term proportional to M_π [8]. Second, the contribution of $N\pi$ and $N\pi\pi$ excited states is expected to be large in $g_S^{u,d}$ [5]. For g_S^s, the leading multihadron excited state is expected to be ΣK, which has a large mass gap, so we consider the "standard" analysis more appropriate for it. A comparison between using the "standard" and $N\pi$ strategies for removing ESC in $g_S^{u,d}$ is shown in Fig. 3 for the physical pion mass ensemble, $a09m130$. The "$N\pi$" analysis gives a 40 $\sim$ 50% larger value. The CC fits are shown in Figs. 6 and 7. To fit the expected chiral behavior in the "$N\pi$" analysis, with at least 2 but likely more M_π-dependent terms contributing significantly, requires data at 5–10 values of M_π. With data at three values ($M_\pi \approx 135, 220, 310$ MeV), even 2 terms in the fit ansatz is an overparametrization as is obvious from Table 3. Our current estimates of g_S^q are summarized in Table 4.

The analysis of $\sigma_{\pi N}$ has been presented recently in Ref. [5] and we reproduce the chiral fits from it in Fig. 8 and the numbers in Table 4. The $N\pi$ analysis gives $\sigma_{\pi N}|_{N\pi} \approx 60$ MeV, consistent with phenomenology while the standard analysis gives a result consistent with previous lattice estimates, $\sigma_{\pi N}|_{\text{standard}} \approx 40$ MeV [5]. For σ_s, we recommend using g_S^s from "without $N\pi$" analyses.

Conclusion: Significant progress has been made in calculating χPT predictions and using them in fits to remove ESC and do the chiral extrapolation. Fits to present data do not, in most

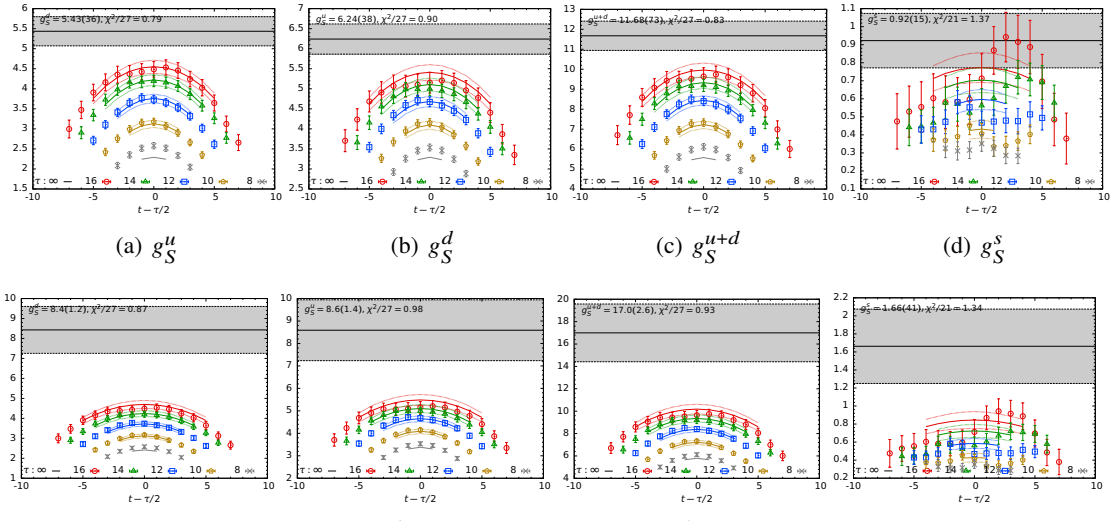

(a) g_S^u (b) g_S^d (c) g_S^{u+d} (d) g_S^s

(e) g_S^u with $N\pi$ (f) g_S^d with $N\pi$ (g) g_S^{u+d} with $N\pi$ (h) g_S^s with $N\pi$

Figure 3: Data for bare g_S from the $a09m130$ ensemble (sum of connected and disconnected contributions) and fits using (i) the "standard" (top) and (ii) the "$N\pi$" (bottom) strategies. The rest is same as in Fig. 2

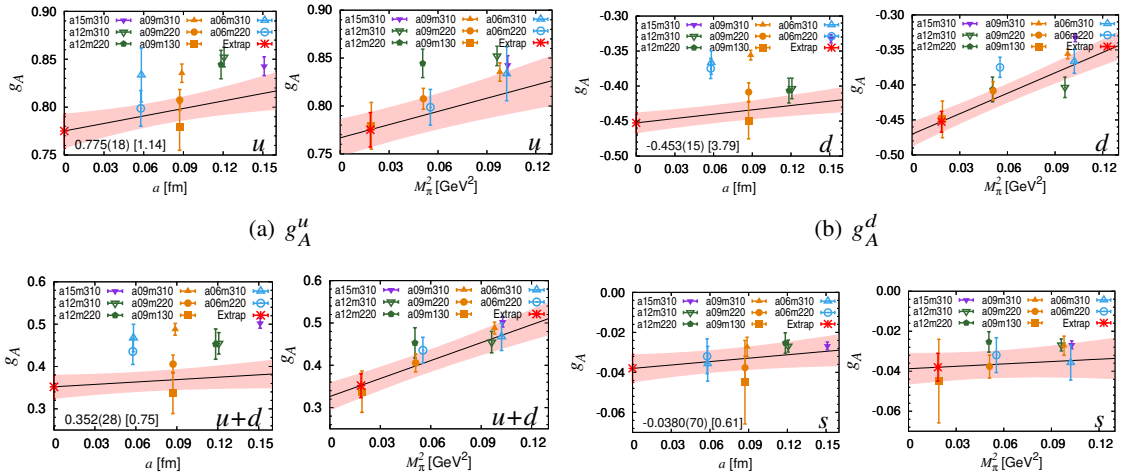

(a) g_A^u (b) g_A^d

(c) g_A^{u+d} (d) g_A^s

Figure 4: Chiral-continuum fits to g_A using the ansatz $d_0 + d_a a + d_2 M_\pi^2$

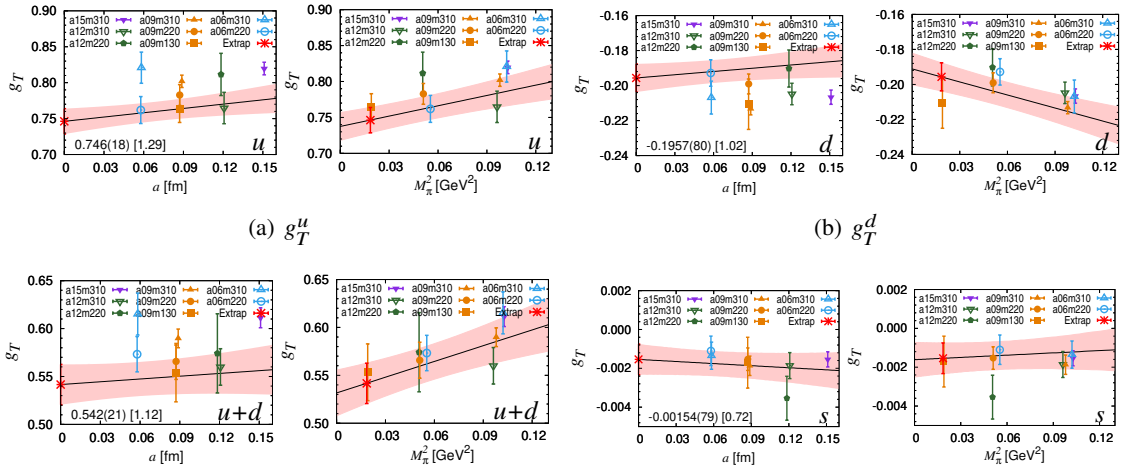

(a) g_T^u (b) g_T^d

(c) g_T^{u+d} (d) g_T^s

Figure 5: Chiral-continuum fits to g_T using the ansatz $d_0 + d_a a + d_2 M_\pi^2$

Fit ansatz	d_0	d_a	d_1	d_2	d_{2L}	$\frac{\chi^2}{dof}$	g_S^{u+d}
$\{a, M_\pi, M_\pi^2\}$	32(10)	−14.0(4.2)	−131(77)	189(144)	–	2.27	17.6(2.4)
$\{a, M_\pi, M_\pi^2, M_\pi^2 \log M_\pi\}$	0.7(48.9)	−15.3(4.6)	447(891)	142(161)	638(979)	2.89	17.1(2.5)
$\{a, M_\pi^2, M_\pi^2 \log M_\pi\}$	25.0(6.0)	−14.3(4.2)	–	184(137)	149(84)	2.23	17.5(2.4)

Table 3: Chiral-Continuum fit coefficients for the renormalized g_S^{u+d} using the ansatz $d_0 + d_a a + d_1 M_\pi + d_2 M_\pi^2 + d_{2L} M_\pi^2 \log M_\pi^2$. Data are from excited states fits assuming the $N\pi$-state contributes.

	g_S^u	g_S^d	g_S^s	$\sigma_{\pi N}$ [MeV] [5]
without $N\pi$	6.29(42)	5.50(39)	0.74(17)	41.9(4.9)
with $N\pi$	9.0(1.3)	8.6(1.1)	1.37(41)	59.6(7.4)

Table 4: Flavor diagonal scalar charges. Results for the pion-nucleon sigma term $\sigma_{\pi N}$ are from Ref. [5].

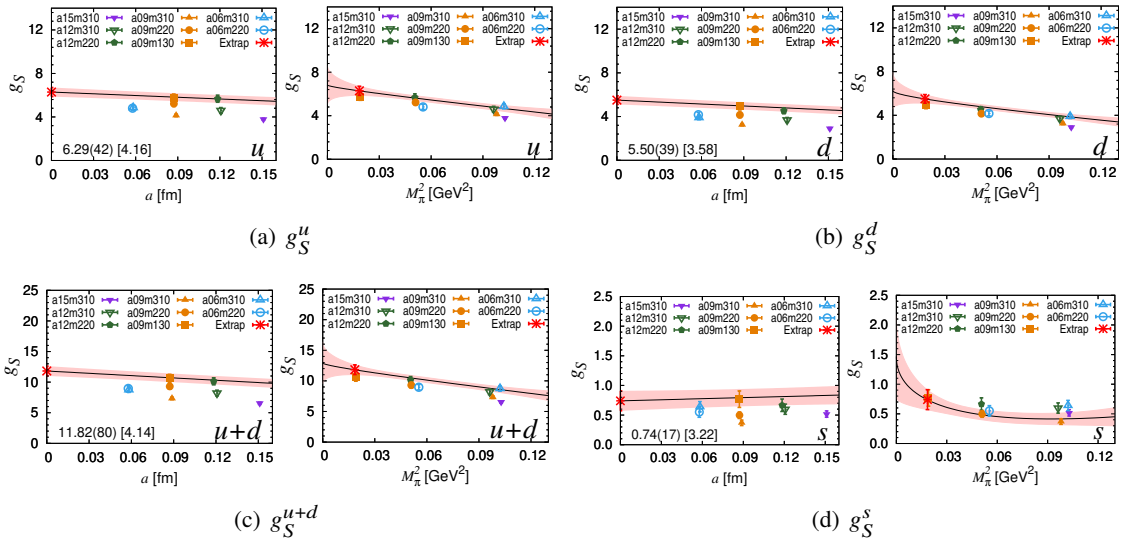

(a) g_S^u (b) g_S^d

(c) g_S^{u+d} (d) g_S^s

Figure 6: Chiral-continuum fits using the ansatz $d_0 + d_a a + d_1 M_\pi + d_2 M_\pi^2$ to g_S from standard analysis.

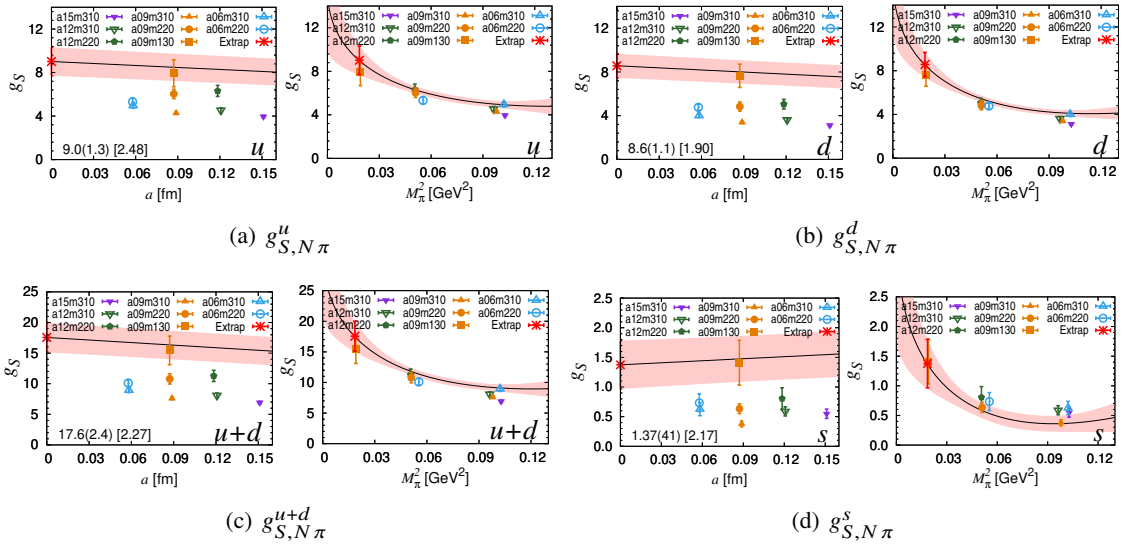

(a) $g^u_{S,N\pi}$ (b) $g^d_{S,N\pi}$

(c) $g^{u+d}_{S,N\pi}$ (d) $g^s_{S,N\pi}$

Figure 7: Chiral-continuum fits using the ansatz $d_0 + d_a a + d_1 M_\pi + d_2 M_\pi^2$ to g_S from $N\pi$ analysis.

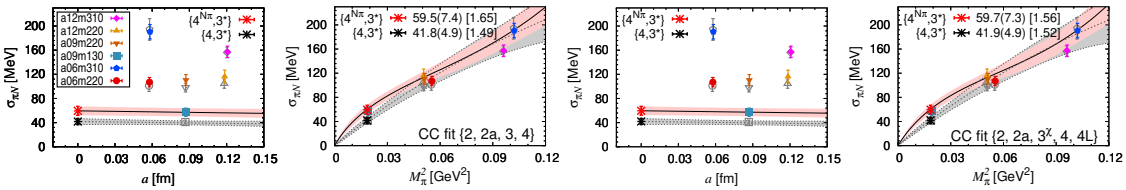

Figure 8: Data for the σ-term, $\sigma_{\pi N} = m_{ud} g_S^{u+d}$, from the two ESC strategies $\{4, 3^*\}$ (gray) and $\{4^{N\pi}, 3^*\}$ (color) are shown as a function of a and M_π^2. These figures, reproduced from Ref. [5], show CC fits $\{2, 2a, 3, 4\}$ (left 2 panels) and $\{2, 2a, 3^\chi, 4, 4L\}$. Final value of $\sigma_{\pi N}$ is given in the legends.

cases, distinguish between standard and $N\pi$ analyses. In the absence of a new methodology, higher statistics data at many more values of M_π and on more physical pion mass ensembles are needed to get percent level estimates for many quantities of phenomenological interest.

5. Acknowledgements

We thank the MILC collaboration for providing the 2+1+1-flavor HISQ lattices. The calculations used the Chroma software suite [9]. This research used resources at (i) the National Energy Research Scientific Computing Center, a DOE Office of Science User Facility supported by the Office of Science of the U.S. Department of Energy under Contract No. DE-AC02-05CH11231; (ii) the Oak Ridge Leadership Computing Facility, which is a DOE Office of Science User Facility supported under Contract DE-AC05-00OR22725, and was awarded through the ALCC program project LGT107; (iii) the USQCD collaboration, which is funded by the Office of Science of the U.S. Department of Energy; and (iv) Institutional Computing at Los Alamos National Laboratory. T. Bhattacharya and R. Gupta were partly supported by the U.S. Department of Energy, Office of Science, Office of High Energy Physics under Contract No. DE-AC52-06NA25396. T. Bhattacharya, R. Gupta, E. Mereghetti, S. Mondal, S. Park, and B. Yoon were partly supported by the LANL LDRD program, and S. Park by the Center for Nonlinear Studies.

References

[1] **MILC** Collaboration, A. Bazavov *et al. Phys. Rev.* **D87** (2013), no. 5 054505, [1212.4768].

[2] R. Gupta, Y.-C. Jang, B. Yoon, H.-W. Lin, V. Cirigliano, and T. Bhattacharya *Phys. Rev.* **D98** (2018) 034503, [1806.09006].

[3] R. Gupta, B. Yoon, T. Bhattacharya, V. Cirigliano, Y.-C. Jang, and H.-W. Lin *Phys. Rev.* **D98** (2018), no. 9 091501, [1808.07597].

[4] H.-W. Lin, R. Gupta, B. Yoon, Y.-C. Jang, and T. Bhattacharya *Phys. Rev.* **D98** (2018), no. 9 094512, [1806.10604].

[5] R. Gupta, S. Park, M. Hoferichter, E. Mereghetti, B. Yoon, and T. Bhattacharya *Phys. Rev. Lett.* **127** (2021), no. 24 242002, [2105.12095].

[6] **PNDME** Collaboration, T. Bhattacharya, V. Cirigliano, S. Cohen, R. Gupta, A. Joseph, H.-W. Lin, and B. Yoon *Phys. Rev.* **D92** (2015), no. 9 094511, [1506.06411].

[7] S. Park, T. Bhattacharya, R. Gupta, Y.-C. Jang, B. Joo, H.-W. Lin, and B. Yoon *PoS* **LATTICE2019** (2020) 136, [2002.02147].

[8] M. Hoferichter, J. Ruiz de Elvira, B. Kubis, and U.-G. Meißner *Phys. Rept.* **625** (2016) 1–88, [1510.06039].

[9] **SciDAC, LHPC, UKQCD** Collaboration, R. G. Edwards and B. Joó *Nucl. Phys. Proc. Suppl.* **140** (2005) 832, [hep-lat/0409003].